J Low Temp Phys (2016) 185:183–197
DOI 10.1007/s10909-016-1515-y

Van Der Waals-Corrected Density Functional Theory Simulation of Adsorption Processes on Noble-Metal Surfaces: Xe on Ag(111), Au(111), and Cu(111)

Pier Luigi Silvestrelli[1,2] · **Alberto Ambrosetti**[1,2]

Received: 16 November 2015 / Accepted: 16 January 2016 / Published online: 1 February 2016

Abstract The DFT/vdW-WF2s1 method based on the generation of localized Wannier functions, recently developed to include the van der Waals interactions in the density functional theory and describe adsorption processes on metal surfaces by taking metal-screening effects into account, is applied to the case of the interaction of Xe with noble-metal surfaces, namely Ag(111), Au(111), and Cu(111). The study is also repeated by adopting the DFT/vdW-QHO-WF variant relying on the quantum harmonic oscillator model which describes well many body effects. Comparison of the computed equilibrium binding energies and distances, and the C_3 coefficients characterizing the adatom–surface van der Waals interactions, with available experimental and theoretical reference data shows that the methods perform well and elucidates the importance of properly including screening effects. The results are also compared with those obtained by other vdW-corrected DFT schemes, including PBE-D, vdW-DF, vdW-DF2, rVV10, and by the simpler local density approximation and semi-local (PBE) generalized gradient approximation approaches.

1 Introduction

Adsorption processes on solid surfaces represent a very important topic both from a fundamental point of view and to design and optimize countless material applications. In particular, the adsorption of rare-gas atoms on metal surfaces is prototypical [1] for ”physisorption” processes, characterized by an equilibrium between attractive,

✉ Pier Luigi Silvestrelli
psil@pd.infn.it

1 Dipartimento di Fisica e Astronomia, Università di Padova, via Marzolo 8, 35131 Padua, Italy

2 DEMOCRITOS National Simulation Center, of the Italian Istituto Officina dei Materiali (IOM) of the Italian National Research Council (CNR), Trieste, Italy

long-range van der Waals (vdW) interactions and short-range Pauli repulsion acting between the electronic charge densities of the substrate and the adsorbed atoms and molecules [2].

Rare-gas adsorption on many close-packed metal surfaces, such as Ag(111), Al(111), Cu(111), Pd(111), Pt(111),.. have been extensively studied both experimentally [3–7] and theoretically [7–16]. Due to the non-directional character of the vdW interactions that should be dominant in physisorption processes, surface sites that maximize the coordination of the rare-gas adsorbate atom are expected to be the preferred ones, thus favoring the *hollow* adsorption site. However, recent studies indicate that the actual scenario is more complex: in particular, for Xe a general tendency is found [7,9–12] for adsorption on metallic surfaces in the low-coordination *top* sites (this behavior is attributed [7,17] to the delocalization of charge density that increases the Pauli repulsion effect at the *hollow* sites relative to the *top* site and lifts the potential well upwards both in energy and height).

Density functional theory (DFT) is a well-established computational approach to study the structural and electronic properties of condensed matter systems from first principles, and, in particular, to elucidate complex surface processes such as adsorptions, catalytic reactions, and diffusive motions. Although current density functionals are able to describe quantitatively condensed matter systems at much lower computational cost than other first-principles methods, they fail [18] to properly describe dispersion interactions. Dispersion forces originate from correlated charge oscillations in separate fragments of matter and the most important component is represented by the R^{-6} vdW interaction [19], originating from correlated instantaneous dipole fluctuations, which plays a fundamental role in adsorption processes of fragments weakly interacting with a substrate ("physisorbed").

This is clearly the case for the present systems which can be divided into well-separated fragments (adatoms and the metal substrate) with negligible electron density overlap. The local or semi-local character of the most commonly employed exchange-correlation functionals makes DFT methods unable to correctly predict binding energies and equilibrium distances within both the local density (LDA) and the generalized gradient approximations (GGA) [20]. Typically, in many physisorbed systems GGAs give only a shallow and flat adsorption well at large adparticle–substrate separations, while the LDA binding energy often turns out to be not far from the experimental adsorption energy; however, since it is well known that LDA tends to overestimate the binding in systems with inhomogeneous electron density (and to underestimate the equilibrium distances), the reasonable performances of LDA must be considered as accidental. Therefore, a theoretical approach beyond the DFT-LDA/GGA framework, that is able to properly describe vdW effects is required to provide more quantitative results [10].

In the last few years a variety of practical methods have been proposed to make DFT calculations able to accurately describe vdW effects (for a recent review, see, for instance, Refs. [20–22]). We have developed a family of such methods, all based on the generation of the maximally localized Wannier functions (MLWFs) [23], successfully applied to a variety of systems, including small molecules, water clusters, graphite and graphene, water layers interacting with graphite, interfacial water on semiconducting substrates, hydrogenated carbon nanotubes, molecular solids, and the interaction of

rare gases and small molecules with metal surfaces [24–37]. Of a particular value is the possibility of dealing with metal surfaces; in fact insulating surfaces could be somehow treated even using atom-based semiempirical approaches where an approximately derived R^{-6} term, multiplied by a suitable short-range damping function, is explicitly introduced. Instead, in our methods the atom-based point of view assumed in standard semiempirical approaches is replaced by an electron-based point of view, so that the schemes are also applicable to systems, such as metals and semimetals, which cannot be described in terms of assemblies of atoms only weakly perturbed with respect to their isolated configuration.

In particular, the DFT/vdW-WF2s1 method, presented in Ref. [35], has been specifically developed to take metal-screening effects into account and has been applied to the study of the adsorption of rare gases and small molecules on different metal surfaces, namely Al(111), Cu(111), and Pb(111), which are systems where a proper inclusion of screening is essential [38]. In fact the vanishing band gap of the metal substrate leads to a fully non-local collective substrate response that effectively screens the interactions, thereby significantly reducing effective C_6 coefficients and polarizability.

The DFT/vdW-QHO-WF variant [36,37] combines the Quantum Harmonic Oscillator (QHO) model with the MLWFs, in such a way to be no longer restricted to the case of well-separated interacting fragments and to include higher than pairwise energy contributions, coming from the dipole–dipole coupling among quantum oscillators. DFT/vdW-QHO-WF hence provides a more complete description of the long-range correlation energy, beyond second-order London dispersion. In particular, the QHO model naturally accounts for non-additive long-range many body effects [36,37], deriving from the self-consistent screening of the system polarizability induced by the Coulomb interaction. In the specific case of adsorption on metal surfaces a long-range damping factor has been introduced [37] to take metal-screening effects into account.

We have already investigated, by the first version of the approach based on the use of the MLWFs, that is the DFT/vdW-WF method [24,25,39], the adsorption of Xe on the Cu(111) and Pb(111) surfaces [32], however in those applications a more crude description of screening effects in metal substrates was adopted.

We here apply our more recent schemes mentioned above, namely DFT/vdW-WF2s1 and DFT/vdW-QHO-WF, to the case of adsorption of Xe on the Ag(111), Au(111), and Cu(111) metal surfaces. Our results will be compared to the best available, reference experimental and theoretical values, and to those obtained by other DFT vdW-corrected schemes, including dispersion-corrected PBE (PBE-D [40,41]), vdW-DF [42–44], vdW-DF2 [45], rVV10 [46] (the revised, more efficient version of the original VV10 scheme [47]), and by the simpler Local Density Approximation (LDA) and semi-local GGA (in the PBE flavor [48]) approaches. In the PBE-D scheme DFT calculations at the PBE level are corrected by adding empirical C_6/R^6 potentials with parameters derived from accurate quantum chemistry calculations for atoms, while in other methods, such as vdW-DF, vdW-DF2, and rVV10, vdW effects are included by introducing DFT non-local correlation functionals.

2 Method

Basically (additional details can be found in Refs. [34,35]), the DFT/vdW-WF2s1 method relies on the well-known London's expression [19] where two interacting atoms, A and B, are approximated by coupled harmonic oscillators and the vdW energy is taken to be the change of the zero-point energy of the coupled oscillations as the atoms approach; if only a single excitation frequency is associated with each atom, ω_A, ω_B, then

$$E_{\mathrm{vdW}}^{\mathrm{London}} = -\frac{3e^4}{2m^2}\frac{Z_A Z_B}{\omega_A \omega_B(\omega_A+\omega_B)}\frac{1}{R_{AB}^6} \tag{1}$$

where $Z_{A,B}$ is the total charge of A and B, and R_{AB} is the distance between the two atoms (e and m are the electronic charge and mass).

Now, adopting a simple classical theory of the atomic polarizability, the polarizability of an electronic shell of charge eZ_i and mass mZ_i, tied to a heavy undeformable ion can be written as

$$\alpha_i \simeq \frac{Z_i e^2}{m\omega_i^2}. \tag{2}$$

Then, given the direct relation between polarizability and atomic volume [49], we assume that $\alpha_i = \gamma S_i^3$, where γ is a proportionality constant, so that the atomic volume is expressed in terms of the MLWF spread, S_i. Rewriting Eq. (1) in terms of the quantities defined above, one obtains an explicit expression for the C_6 vdW coefficient:

$$C_6^{AB} = \frac{3}{2}\frac{\sqrt{Z_A Z_B}S_A^3 S_B^3 \gamma^{3/2}}{(\sqrt{Z_B}S_A^{3/2}+\sqrt{Z_A}S_B^{3/2})}. \tag{3}$$

The constant γ can then be set up by imposing that the exact value for the H atom polarizability (α_H =4.5 a.u.) is obtained; of course, in the H case, one knows the exact analytical spread, $S_i = S_H = \sqrt{3}$ a.u.

In order to achieve a better accuracy, one must properly deal with *intrafragment* MLWF charge overlap. This overlap affects the effective orbital volume, the polarizability, and the excitation frequency [see Eq. (2)], thus leading to a quantitative effect on the value of the C_6 coefficient. We take into account the effective change in volume due to intrafragment MLWF overlap by introducing a suitable reduction factor ξ obtained by interpolating between the limiting cases of fully overlapping and non-overlapping MLWFs (see Ref. [34]). We therefore arrive at the following expression for the C_6 coefficient:

$$C_6^{AB} = \frac{3}{2}\frac{\sqrt{Z_A Z_B}\xi_A S_A^3 \xi_B S_B^3 \gamma^{3/2}}{(\sqrt{Z_B \xi_A}S_A^{3/2}+\sqrt{Z_A \xi_B}S_B^{3/2})}, \tag{4}$$

where $\xi_{A,B}$ represents the ratio between the effective and the free volume associated with the A-th and B-th MLWF.

Finally, the vdW interaction energy is computed as:

$$E_{\mathrm{vdW}} = -\sum_{i<j} f(R_{ij}) \frac{C_6^{ij}}{R_{ij}^6}, \tag{5}$$

where $f(R_{ij})$ is a short-range damping function defined as follows:

$$f(R_{ij}) = \frac{1}{1 + e^{-a(R_{ij}/R_s - 1)}}. \tag{6}$$

This short-range damping function is introduced not only to avoid the unphysical divergence of the vdW correction at small fragment separations, but also to eliminate double countings of correlation effects, by considering that standard DFT approaches properly describe short-range correlations.

The parameter R_s represents the sum of the vdW radii $R_s = R_i^{\mathrm{vdW}} + R_j^{\mathrm{vdW}}$, with (by adopting the same criterion chosen above for the γ parameter)

$$R_i^{\mathrm{vdW}} = R_H^{\mathrm{vdW}} \frac{S_i}{\sqrt{3}}, \tag{7}$$

where R_H^{vdW} is the literature [50] (1.20 Å) vdW radius of the H atom, and, following Grimme *et al.* [51,52], $a \simeq 20$; note that the results are only mildly dependent on the particular value of this parameter, at least within a reasonable range around the $a = 20$ value: for instance, the binding energy at the optimal Xe–Ag(111) distance changes by less than 5% by varying a between 10 and 30. Although the damping function introduces a certain degree of empiricism in the method, we stress that a is the only ad-hoc parameter present in our approach, while all the others are only determined by the basic information given by the MLWFs, namely from first-principles calculations so that they adapt to the specific chemical environment.

To get an appropriate inclusion of metal-screening effects a proper reduction coefficient is included by multiplying the C_6^{ij}/R_{ij}^6 contribution in Eq. (5) by a Thomas–Fermi factor: $f_{\mathrm{TF}} = e^{-2(z_s - z_l)/r_{\mathrm{TF}}}$, where r_{TF} is the Thomas–Fermi screening length relative to the electronic density of an effective uniform electron gas ("jellium model") describing the substrate, z_s is the average vertical position of the topmost metal atoms, and z_l is the vertical coordinate of the Wannier function center (WFC) belonging to the substrate ($l = i$ if it is the i-th WFC which belongs to the substrate, otherwise $l = j$); the above f_{TF} function is only applied if $z_l < z_s$, otherwise it is assumed that $f_{\mathrm{TF}} = 1$ (no screening effect).

An alternative, even simpler approach to mimic screening effects in adsorption processes is represented by the so-called "single-layer" approximation, in which vdW effects are only restricted to the interactions of the adparticle with the topmost metal layer [53]; in fact, as a consequence of screening, one expects that the topmost metal atoms give the dominant contribution. We have implemented this by multiplying the C_6^{ij}/R_{ij}^6 factor in Eq. (5) by a damping function:

$$f_{SL} = 1 - \frac{1}{1 + e^{(z_l - z_r)/\Delta z}} , \tag{8}$$

where z_l is the vertical coordinate of the WFC belonging to substrate (again $l = i$ if it is the i-th WFCs which belongs to the substrate, otherwise $l = j$), the reference level z_r is taken as an intermediate between the level of the first, topmost surface layer, and the second one, and we assume that Δz =(interlayer separation)/4; we found that the estimated equilibrium binding energies and adparticle–surface distances exhibit only a mild dependence on the Δz parameter. Clearly this approach, denoted as DFT/vdW-WF2s3 [35], resembles the DFT/vdW-WF2s1 scheme, the basic difference being that the Thomas–Fermi damping function of DFT/vdW-WF2s1 is here replaced by the f_{SL} damping function introduced to just select the WFCs around the topmost surface layer.

In the DFT/vdW-QHO-WF variant (further details can be found in Refs. [36,37]) one exploits instead the fact that for a system of N three-dimensional QHOs the exact total energy can be obtained [54–59] by diagonalizing the $3N \times 3N$ matrix C^{QHO}, containing N^2 blocks C_{ij}^{QHO} of size 3×3:

$$C_{ii}^{\mathrm{QHO}} = \omega_i^2 \mathbf{I}; \quad C_{i \neq j}^{\mathrm{QHO}} = \omega_i \omega_j \sqrt{\alpha_i \alpha_j} T_{ij}, \tag{9}$$

where $\mathbf{I}$ is the identity matrix, T_{ij} is the dipole–dipole interaction tensor, and ω_i and α_i are the characteristic frequency and the static dipole polarizability, respectively, of the i-th oscillator. The interaction (correlation) energy is given by the difference between the ground state energy of the *coupled* system of QHOs (proportional to the square root of the eigenvalues λ_p of the C^{QHO} matrix) and the ground state energy of the *uncoupled* system of QHOs (derived from the characteristic frequencies):

$$E_{c,\mathrm{QHO}} = 1/2 \sum_{p=1}^{3N} \sqrt{\lambda_p} - 3/2 \sum_{i=1}^{N} \omega_i \, . \tag{10}$$

The so-computed interaction energy naturally includes many body energy contributions, due to the dipole–dipole coupling among the QHOs; moreover, it can be proved [58,59] that the QHO model provides an efficient description of the correlation energy for a set of localized fluctuating dipoles at an effective random phase approximation (RPA) level. This is important because, differently from other schemes, RPA includes the effects of long-range screening of the vdW interactions [60], which are clearly of relevance, particularly for extended systems [22,61,62]. The QHO interaction energy accounts for the long-range component of the correlation energy, and is added to the energy computed within the underlying semi-local DFT approximation. Due to the short-range character of semi-local functionals (PBE in our case), this procedure avoids double counting of the correlation energy since a proper short-range damped form of the QHO interaction is used.

The QHO model can be combined with the MLWF technique by assuming that each MLWF is represented by a three-dimensional isotropic harmonic oscillator, so that the system is described as an assembly of fluctuating dipoles. By considering [58,59] the

Coulomb interaction between two spherical Gaussian charge densities to account for orbital overlap at short distances (thus introducing a short-range damping):

$$V_{ij} = \frac{\mathrm{erf}(r_{ij}/\sigma_{ij})}{r_{ij}}\,, \tag{11}$$

where r_{ij} is the distance between the i-th and the j-th Wannier function center (WFC), and σ_{ij} is an effective width, $\sigma_{ij} = \sqrt{S_i^2 + S_j^2}$, where S_i is the spread of the i-th MLWF, w_i; S_i^2 is defined as $\langle w_i|r^2|w_i\rangle - \langle w_i|\mathbf{r}|w_i\rangle^2$. Then, in Eq. (9) the dipole interaction tensor is [58,59]

$$T_{ij}^{ab} = -\frac{3r_{ij}^a r_{ij}^b - r_{ij}^2\delta_{ab}}{r_{ij}^5}\left(\mathrm{erf}\left(\frac{r_{ij}}{\sigma_{ij}}\right) - \frac{2}{\sqrt{\pi}}\frac{r_{ij}}{\sigma_{ij}}e^{-\left(\frac{r_{ij}}{\sigma_{ij}}\right)^2}\right) + \frac{4}{\sqrt{\pi}}\frac{1}{\sigma_{ij}^3}\frac{r_{ij}^a r_{ij}^b}{r_{ij}^2}e^{-\left(\frac{r_{ij}}{\sigma_{ij}}\right)^2}\,, \tag{12}$$

where a and b specify Cartesian coordinates (x, y, z), r_{ij}^a and r_{ij}^b are the respective components of the distance r_{ij}, and δ_{ab} is the Kronecker delta function.

Moreover, similar to Eq. (2), the polarizability is written as

$$\alpha_i = \zeta\frac{Z_i e^2}{m\omega_i^2}\,, \tag{13}$$

where, if spin degeneracy is exploited, $Z_i = 2$ since every MLWF corresponds to two paired electrons. Then, given again the direct relation between polarizability and volume, we assume that $\alpha_i = \gamma S_i^3$.

Similar to refs. [36,37], we combine the QHO model, which accurately describes the long-range correlation energy, with a given semi-local, GGA functional (PBE in our case), which is expected to well reproduce short-range correlation effects, by introducing an empirical parameter β that multiplies the QHO–QHO parameter σ_{ij} in Eq. (11). The three parameters β, γ, and ζ are set up by minimizing the mean absolute relative errors (MARE), measured with respect to high-level, quantum chemistry reference values relative to the S22 database of intermolecular interactions [63], a widely used benchmark database, consisting of weakly interacting molecules (a set of 22 weakly interacting dimers mostly of biological importance), with reference binding energies calculated by a number of different groups using high-level quantum chemical methods. By taking PBE as the reference DFT functional, we get: $\beta = 1.39$, $\gamma = 0.88$, and $\zeta = 1.30$ [36]. Once the γ and ζ parameters are set up, both the polarizability α_i and the characteristic frequency ω_i are obtained just in terms of the MLWF spreads [see Eq. (13) and below].

As in Ref. [36], in order to describe screening effects in the metal substrate, the potential of Eq. (11) is replaced by

$$V_{ij} = \frac{\mathrm{erf}(r_{ij}/\sigma_{ij})\,e^{-qr_{ij}}}{r_{ij}}\,, \tag{14}$$

where q is the standard Thomas–Fermi wave vector, k_{TF}, appropriate for the substrate bulk metal if both the i-th and the j-th WFC are inside the metal slab, $q = 0$ if both the WFCs are outside the metal slab, while, in the intermediate cases, $q = k_{\mathrm{TF}}\, r_{ij}^{in}/r_{ij}$, that is k_{TF} is renormalized by considering the portion, r_{ij}^{in}, of the r_{ij} segment which is inside the metal slab.

In this way the method includes both a short-range damping (to take orbital overlap effects into account) and a long-range damping (to take metal-screening effects into account).

2.1 Computational Details

We here apply the DFT/vdW-WF2s1, DFT/vdW-WF2s3, and DFT/vdW-QHO-WF methods to the case of adsorption of Xe on the Ag(111), Au(111), and Cu(111) metal surfaces. All calculations have been performed with the Quantum ESPRESSO ab initio package [64] and the MLWFs have been generated as a post-processing calculation using the WanT package [65,66]. Similar to our previous studies [32,35] we modeled the metal surface using a periodically repeated hexagonal supercell, with a $(\sqrt{3} \times \sqrt{3})R30°$ structure and a surface slab made of 15 metal atoms distributed over 5 layers considering the experimental Ag(111), Au(111), and Cu(111) lattice constants. Repeated slabs were separated along the direction orthogonal to the surface by a vacuum region of about 20 Å to avoid significant spurious interactions due to periodic replicas. The Brillouin Zone has been sampled using a $6 \times 6 \times 1$ k-point mesh. In this model system the coverage is 1/3, i.e., one adsorbed adatom for each 3 metal atoms in the topmost surface layer. The $(\sqrt{3} \times \sqrt{3})R30°$ structure has been indeed observed [4,5] at low temperature by LEED for the case of Xe adsorption on Cu(111) and Pd(111) (actually, this is the simplest commensurate structure for rare-gas monolayers on close-packed metal surfaces and the only one for which good experimental data exist), and it was adopted in most of the previous ab initio studies [8–10,12,13,67]. The metal surface atoms were kept frozen (after a preliminary relaxation of the outermost layers of the clean metal surfaces) and only the vertical coordinate (perpendicular to the surface) of the adatoms was optimized, this procedure being justified by the fact that only minor surface atom displacements are observed upon physisorption [9,67–69]. Moreover, the adatoms were adsorbed on both sides of the slab: in this way the surface dipole generated by adsorption on the upper surface of the slab is canceled by the dipole appearing on the lower surface, thus greatly reducing the spurious dipole–dipole interactions between the periodically repeated images (previous DFT-based calculations have shown that these choices are appropriate [10,14,32,70]).

We have carried out calculations for various separations of the Xe atoms adsorbed on the *top* high-symmetry site (on the top of a metal atom), since this is certainly the favored adsorption site for Xe [32,71–75]. For the Xe–Ag(111) system we have also considered adsorption on the *hollow* site (on the center of the triangle formed by the 3 surface metal atoms contained in the supercell) in order to verify whether the present schemes are able to correctly predict which configuration is energetically favored (see discussion in Ref. [32]).

In principle the adsorption on metal surfaces is challenging for a Wannier-based scheme since in metal slabs the electronic charge is relatively delocalized [76] and the assumption of exponential localization of the MLWFs is no longer strictly valid [77–79]. However, even in this case our methods perform well, as confirmed by the fact that the spreads of our computed MLWFs are not larger than 2.5 Å for the systems we have considered, so that the MLWFs are relatively localized although the total electronic density is certainly not. This does not come to a surprise; in fact, on the one hand, the MLWF technique has been efficiently generalized also to metals [80,81], on the other, bonding in metallic clusters and in fcc bulk metals (like Ag, Au, and Cu) can be described in terms of Hydrogen-like orbitals localized on tetrahedral interstitial sites [80], which is just in line with the spirit of our vdW-corrected schemes based on MLWFs.

For a better accuracy, as done in previous applications on adsorption processes [25,26,28,29,32], we have also included the interactions of the MLWFs of the physisorbed fragments not only with the MLWFs of the underlying surface, within the reference supercell, but also with a sufficient number of periodically repeated surface MLWFs (in any case, given the R^{-6} decay of the vdW interactions, the convergence with the number of repeated images is rapidly achieved). Electron–ion interactions were described using ultrasoft pseudopotentials by explicitly including 11 valence electrons per Ag, Au, and Cu atom. We chose the PBE [48] reference DFT functional, which is probably the most popular GGA functional. The problem of choosing the optimal DFT functional, particularly in its exchange component, to be combined with long-range vdW interactions and the related problem of completely eliminating double counting of correlation effects still remain open [20]; however they are expected to be more crucial for adsorption systems characterized by relatively strong adparticle–substrate bonds ("chemisorption") and, for instance, for the determination of the perpendicular vibration frequency [12] than for the equilibrium properties of the physisorbed systems we focus on in our paper.

The additional cost of the post-processing vdW correction is basically represented by the cost of generating the Maximally Localized Wannier functions from the Kohn–Sham orbitals, which scales linearly with the size of the system [23].

3 Results and Discussion

In Tables 1, 2, 3 and Fig. 1 we report results evaluated including the vdW corrections using our screened DFT/vdW-WF2s1 and DFT/vdW-QHO-WF methods, and DFT/vdW-WF2, namely the unscreened version of DFT/vdW-WF2s1. We also add data obtained by the simple, single-layer DFT/vdW-WF2s3 scheme (see Sect. 2). Our estimated binding energies and equilibrium distances are compared (see Table 1) to the best available, reference experimental and theoretical values, and to those obtained by other DFT vdW-corrected schemes, including dispersion-corrected PBE (PBE-D [40,41]), vdW-DF [42–44], vdW-DF2 [45], rVV10 [46], and by the simpler local density approximation (LDA) and semi-local GGA (in the PBE flavor [48]) approaches. For the Xe–Ag(111) case we also report recent data computed by the PBE + vdW$^{\text{surf}}$ [82], PBE + MBD [82], and cRPA + EXX [83] methods.

Table 1 Binding energy per Xe atom E_b (in meV) and (in parenthesis) equilibrium distance R (in Å) for Xe adsorbed on Ag(111), Au(111), and Cu(111) metal surfaces in the *top* configuration, using different methods. Results are compared with available reference data.

Method	Xe–Ag (111)	Xe–Au (111)	Xe–Cu (111)
LDA	−215 (3.12)	−230 (3.14)	−204 (3.04)
PBE	−18 (5.02)	−19 (4.34)	−19 (4.49)
PBE-D	−282 (3.54)	−517 (3.22)	−272 (3.40)
rVV10	−236 (3.53)	−280 (3.48)	−223 (3.47)
vdW-DF	−180 (4.08)	−199 (4.00)	−184 (3.97)
vdW-DF2	−154 (4.00)	−180 (3.86)	−157 (4.01)
PBE+vdW^{surf}	−220 (3.56)[a]	–	–
PBE+MBD	−170 (3.64)[a]	–	–
cRPA+EXX	−140 (3.60)[b]	–	–
DFT/vdW-WF2	−298 (3.13)	−277 (3.36)	−304 (3.11)
DFT/vdW-WF2s1	−186 (3.34)	−209 (3.42)	−189 (3.24)
DFT/vdW-WF2s3	−179 (3.37)	−197 (3.44)	−197 (3.23)
DFT/vdW-QHO-WF	−199 (3.45)	−227 (3.49)	−188 (3.28)
Reference	−230↔−180 (3.45↔3.68)[c]	−214[d]	−280↔−183 (3.20↔4.00)[d,e]
"Best estimate"[d]	−211±15(3.60±5)	—	−183 ± 10 (3.60)

[a]Ref. [82]
[b]Ref. [83]
[c]Ref. [85–89]
[d]Ref. [2]
[e]Refs. [4,12,15]

Table 2 Binding energy per Xe atom E_b (in meV) and (in parenthesis) equilibrium distance R (in Å) for Xe adsorbed on Ag(111) in the *top* and *hollow* configurations, using different methods.

Method	Top	Hollow
LDA	−215 (3.12)	−205 (3.07)
PBE	−18 (5.02)	−18 (4.22)
PBE-D	−282 (3.54)	−317 (3.38)
rVV10	−236 (3.53)	−234 (3.52)
vdW-DF	−180 (4.08)	−179 (4.08)
vdW-DF2	−154 (4.00)	−152 (4.01)
DFT/vdW-WF2	−298 (3.13)	−246 (3.24)
DFT/vdW-WF2s1	−186 (3.34)	−175 (3.31)
DFT/vdW-WF2s3	−179 (3.37)	−167 (3.40)
DFT/vdW-QHO-WF	−199 (3.45)	−198 (3.46)

The *binding energy*, E_b, is defined as

$$E_b = 1/2\,(E_{\text{tot}} - (E_s + 2E_a))\,, \tag{15}$$

where $E_{s,a}$ represent the energies of the isolated fragments (the substrate and the adatoms) and E_{tot} is the energy of the interacting system, including the vdW correction

Table 3 Estimated C_3 coefficients, in eVÅ^3, for Xe in the *top* configuration on the metal surfaces computed using data obtained by our methods (by fitting the binding energy curve, see text), compared to available reference data.

Method	Xe–Ag (111)	Xe–Au (111)	Xe–Cu (111)
DFT/vdW-WF2	3.29	5.59	5.84
DFT/vdW-WF2s1	3.30	4.30	4.25
DFT/vdW-WF2s3	3.41	4.11	4.38
DFT/vdW-QHO-WF	4.62	5.59	4.92
reference [a]	3.28	3.20↔3.79	3.39

[a]Ref. [2].

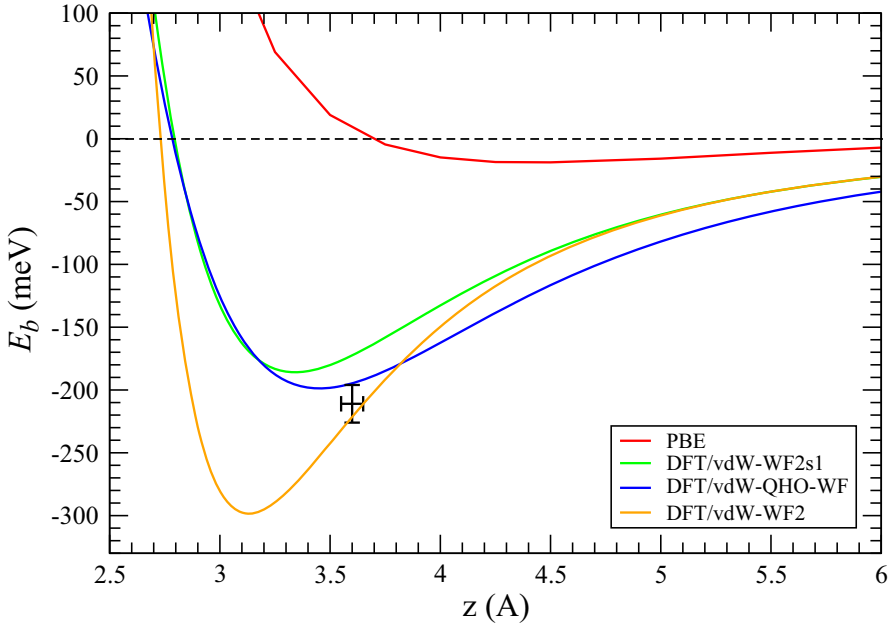

Fig. 1 Binding energy of Xe on Ag(111), as a function of the distance from the Ag(111) surface, computed using the standard PBE calculation, and including the vdW corrections using our (unscreened) DFT/vdW-WF2, and (screened) DFT/vdW-WF2s1, and DFT/vdW-QHO-WF methods; the position of the "best estimate" value [2] with error bars is also reported (Color figure online)

term (the factors 2 and 1/2 are due to the adsorption on both sides of the slab); E_s and E_a are evaluated using the same supercell adopted for $E_{\rm tot}$.

E_b has been evaluated for several adsorbate–substrate distances; then the equilibrium distances and the corresponding binding energies have been obtained (as in Refs. [32,35]) by fitting the calculated points with the function: $A\,e^{-Bz} - C_3/(z-z_0)^3$ (plotted in Fig. 1 for the Xe–Ag(111) case; the Xe–Au(111) and the Xe–Cu(111) binding energies look very similar). Typical uncertainties in the fit are of the order of 0.05 Å for the distances and a few meVs for the minimum binding energies. For the adsorption of rare gases on the (111) noble-metal surface, reference data are available, particularly

the "best estimates" reported by Vidali et al. [2], that represent averages over different theoretical and experimental evaluations.

As found in the previous studies [32,35] the effect of the vdW-corrected schemes (see Table 1 and Fig. 1) is a much stronger bonding than with a pure PBE scheme (PBE yielding no significant binding), with the formation of a clear minimum in the binding energy curve at a shorter equilibrium distance. Moreover, by comparing with unscreened DFT/vdW-WF2 data, we see that the effect of screening is substantial, leading to reduced binding energies and increased adatom–substrate equilibrium distances: the unscreened approach evidently overbinds. With respect to the reference values, our screened methods appear to well reproduce the equilibrium binding energies, although the equilibrium distances are slightly shorter.

All the considered theoretical schemes (see Table 2) predict that the *top* site is favored with respect to the *hollow* one for Xe on Ag(111) (in agreement with the experimental evidence [7]), with the exception of PBE-D, thus confirming that employing a semiempirical approach is inappropriate for such a system. PBE predicts that the *top* and *hollow* configurations are essentially isoenergetic since the equilibrium Xe–Ag(111) distance is largely overestimated and the bonding strength largely underestimated. Note also that with the unscreened DFT/vdW-WF2 approach the difference between the binding energies of the *top* and *hollow* structures is substantially overestimated. Interestingly, for the systems considered, the simple DFT/vdW-WF2s3 scheme, based on the single-layer approximation also performs well.

The slight underestimate of our binding energies compared to the "best estimates" values [2] could also be rationalized by considering that the experimentally measured adsorption energy often includes not only the interaction of adatoms with the substrate but also lateral interactions among adatoms [14,32], thus leading to higher energy estimates.

Concerning the other vdW-corrected methods considered, PBE-D gives reasonable equilibrium distances but largely overbinds (much more than LDA), particularly for the Xe–Au(111) where the error is of more than 100 %. This bad performance is not unexpected since such a semiempirical, atom-based approach cannot well describe metal substrates with their delocalized electronic charge and screening effects. rVV10 gives reasonable equilibrium distances but tends to overbind (more than LDA), while vdW-DF and vdW-DF2, as expected [22] for this kind of vdW functionals, substantially overestimate the equilibrium adsorption distances, with vdW-DF2 which also turns out to significantly underestimate the binding energy.

From Table 1 one can also see that the binding energies are reasonably reproduced by the LDA scheme for the all cases, a behavior common to several physisorption systems. However, as already outlined above, this agreement should be considered accidental: the well-known LDA overbinding, due to the overestimate of the long-range part of the exchange contribution, somehow mimics the missing vdW interactions; moreover the equilibrium distances predicted by LDA are clearly underestimated since LDA cannot reproduce the R^{-6} behavior in the interaction potential, so that the binding energy exhibits a wrong asymptotic behavior at a large distance Z from the surface (decaying exponentially rather than as $\sim 1/Z^3$).

Looking at data for the Xe–Ag(111) system, one can also see the relatively good performances of the PBE + vdW$^{\text{surf}}$ and PBE+MBD methods [82]. The underbind-

ing exhibited by the cRPA-EXX calculation of Ref. [83], which combines exact exchange and random phase approximation (RPA) correlation without using any density functional, is probably due [82] to neglect of the exchange-correlation kernel, the underlying plasmon-pole approximation, and the fact that the response function of the system is not fully coupled, being calculated separately for substrate and adsorbate.

As can be seen from Table 1, the values of the binding energies of Xe on Ag(111), Au(111), and Cu(111) are comparable, with Xe–Au(111) which turns out to be the system which is energetically slightly more favored according to most of the vdW-corrected schemes. Interestingly, using the unscreened DFT/vdW-WF2 method the Xe–Au(111) is instead the least energetical system, thus confirming once again the importance of screening effects in the adsorption processes on metal surfaces.

Concerning the computed C_3 coefficients (see Table 3) using data obtained by our methods and fitting the binding energy curve, they appear in reasonable, semiquantitative agreement with reference data [particularly for the Xe–Ag(111) system], although one should remember that our estimated values cannot be very accurate given the limited size of our simulation slab and vacuum thickness (as discussed, for instance, in Ref. [83]).

4 Conclusions

In summary, we have investigated the adsorption of Xe on the Ag(111), Au(111), and Cu(111) metal surfaces, by considering our screened DFT/vdW-WF2s1, DFT/vdW-WF2s3, and DFT/vdW-QHO-WF methods. By analyzing the results of our study and comparing them to available reference data, we get a substantial improvement with respect to the unscreened DFT/vdW-WF2 approach. Given the uncertainties in the reference data, one cannot easily state which scheme is more appropriate. Considering all the studied cases DFT/vdW-QHO-WF turns out to be marginally superior which correlates with the relatively higher complexity of this approach. Interestingly, we confirm the conclusion of previous studies (see, Ref. [53] and references therein) which suggest that, particularly for the close-packed (111) surfaces, the assumption of a one-layer screening depth (single-layer approximation) works reasonably well (DFT/vdW-WF2s3 approach). The differences between the values of the equilibrium binding energies and distances predicted by our adopted different schemes can be taken as the order of magnitude of the uncertainty associated with the different screened methods and to estimate their accuracy.

For the considered systems, in general our methods are comparable with the most recent vdW-corrected schemes, such as PBE+vdW$^{\text{surf}}$ and PBE+MBD; moreover they perform better than the semiempirical PBE-D method and the popular vdW-DF and vdW-DF2 approaches, which, in particular, exhibit a general tendency to overestimate the equilibrium distances, in line with the behavior reported for systems including a metallic surface [84].

References

1. L.W. Bruch, M.W. Cole, E. Zaremba, *Physical Adsorption: Forces and Phenomena* (Clarendon Press, Oxford, 1997)

2. G. Vidali, G. Ihm, H.Y. Kim, M.W. Cole, Surf. Sci. Rep. **12**, 133 (1991)
3. J.M. Gottlieb, Phys. Rev. B **42**, 5377 (1990)
4. M. Th Seyller, R.D. Caragiu, P. Diehl, M.Lindroos Kaukasoina, Chem. Phys. Lett. **291**, 567 (1998)
5. M. Caragiu, T. Seyller, R.D. Diehl, Phys. Rev. B **66**, 195411 (2002)
6. B. Narloch, D. Menzel, Chem. Phys. Lett. **290**, 163 (1997)
7. R.D. Diehl, M. Th Seyller, G.S. Caragiu, N. Leatherman, K. Ferralis, P. Pussi, M.Lindroos Kaukasoina, J. Phys. **16**, S2839 (2004)
8. J.L.F. Da Silva, C. Stampfl, M. Scheffler, Phys. Rev. Lett. **90**, 066104 (2003)
9. J.L.F. Da Silva, C. Stampfl, M. Scheffler, Phys. Rev. B **72**, 075424 (2005)
10. J.L.F. Da Silva, C. Stampfl, Phys. Rev. B **77**, 045401 (2008)
11. A.E. Betancourt, D.M. Bird, J. Phys. **12**, 7077 (2000)
12. P. Lazić, Ž. Crljen, R. Brako, B. Gumhalter, Phys. Rev. B **72**, 245407 (2005)
13. M.C. Righi, M. Ferrario, J. Phys. **19**, 305008 (2007)
14. X. Sun, Y. Yamauchi, J. Appl. Phys. **110**, 103701 (2011)
15. D.-L. Chen, W.A. Al-Saidi, J.K. Johnson, Phys. Rev. B **84**, 241405(R) (2011)
16. D.-L. Chen, W.A. Al-Saidi, J.K. Johnson, J. Phys. **24**, 424211 (2012)
17. P.S. Bagus, V. Staemmler, C. Wöll, Phys. Rev. Lett. **89**, 096104 (2002)
18. W. Kohn, Y. Meir, D.E. Makarov, Phys. Rev. Lett. **80**, 4153 (1998)
19. R. Eisenhitz, F. London, Z. Phys. **60**, 491 (1930)
20. K.E. Riley, M. Pitoňák, P. Jurečka, P. Hobza, Chem. Rev. **110**, 5023 (2010)
21. A. Tkatchenko, L. Romaner, O.T. Hofmann, E. Zojer, C. Ambrosch-Draxl, M. Scheffler, MRS Bulletin **35**, 435 (2010)
22. J. Klimeš, A. Michaelides, J. Chem. Phys. **137**, 120901 (2012)
23. N. Marzari, D. Vanderbilt, Phys. Rev. B **56**, 12847 (1997)
24. P.L. Silvestrelli, Phys. Rev. Lett **100**, 053002 (2008)
25. P.L. Silvestrelli, J. Phys. Chem. A **113**, 5224 (2009)
26. P.L. Silvestrelli, K. Benyahia, S. Grubisiĉ, F. Ancilotto, F. Toigo, J. Chem. Phys. **130**, 074702 (2009)
27. P.L. Silvestrelli, Chem. Phys. Lett. **475**, 285 (2009)
28. P.L. Silvestrelli, F. Toigo, F. Ancilotto, J. Phys. Chem. C **113**, 17124 (2009)
29. A. Ambrosetti, P.L. Silvestrelli, J. Phys. Chem. C **115**, 3695 (2011)
30. F. Costanzo, P.L. Silvestrelli, F. Ancilotto, J. Chem. Theory Comp. **8**, 1288 (2012)
31. F. Costanzo, P.L. Silvestrelli, F. Ancilotto, Arch. Metall. Mater. **57**, 1075 (2012)
32. P.L. Silvestrelli, A. Ambrosetti, S. Grubisiĉ, F. Ancilotto, Phys. Rev. B **85**, 165405 (2012)
33. A. Ambrosetti, F. Ancilotto, P.L. Silvestrelli, J. Phys. Chem. C **117**, 321 (2013)
34. A. Ambrosetti, P.L. Silvestrelli, Phys. Rev. B **85**, 073101 (2012)
35. P.L. Silvestrelli, A. Ambrosetti, Phys. Rev. B **87**, 075401 (2013)
36. P.L. Silvestrelli, J. Chem. Phys. **139**, 054106 (2013)
37. P.L. Silvestrelli, A. Ambrosetti, J. Chem. Phys. **140**, 124107 (2014)
38. V.G. Ruiz, W. Liu, E. Zojer, M. Scheffler, A. Tkatchenko, Phys. Rev. Lett. **108**, 146103 (2012)
39. L. Andrinopoulos, N.D.M. Hine, A.A. Mostofi, J. Chem. Phys. **135**, 154105 (2011)
40. S. Grimme, J. Comp. Chem. **27**, 1787 (2006)
41. V. Barone, M. Casarin, D. Forrer, M. Pavone, M. Sambi, A. Vittadini, J. Comp. Chem. **30**, 934 (2009)
42. M. Dion, H. Rydberg, E. Schröder, D.C. Langreth, B.I. Lundqvist, Phys. Rev. Lett. **92**, 246401 (2004)
43. G. Roman-Perez, J.M. Soler, Phys. Rev. Lett. **103**, 096102 (2009)
44. T. Thonhauser, V.R. Cooper, S. Li, A. Puzder, P. Hyldgaard, D.C. Langreth, Phys. Rev. B **76**, 125112 (2007)
45. K. Lee, É.D. Murray, L. Kong, B.I. Lundqvist, D.C. Langreth, Phys. Rev. B **82**, 081101(R) (2010)
46. R. Sabatini, T. Gorni, S. de Gironcoli, Phys. Rev. B **87**, 041108(R) (2013)
47. O.A. Vydrov, T. Van Voorhis, J. Chem. Phys. **133**, 244103 (2010)
48. J.P. Perdew, K. Burke, M. Ernzerhof, Phys. Rev. Lett. **77**, 3865 (1996)
49. T. Brink, J.S. Murray, P. Politzer, J. Chem. Phys. **98**, 4305 (1993)
50. A. Bondi, J. Phys. Chem. **68**, 441 (1964)
51. S. Grimme, J. Antony, T. Schwabe, C. Mück-Lichtenfeld, Org. Biomol. Chem. **5**, 741 (2007)
52. S. Grimme, J. Antony, S. Ehrlich, H. Krieg, J. Chem. Phys. **132**, 154104 (2010)
53. F. Hanke, M.S. Dyer, J. Biörk, M. Persson, J. Phys. **24**, 424217 (2012)
54. J. Cao, B.J. Berne, J. Chem. Phys. **97**, 8628 (1992)
55. A.G. Donchev, J. Chem. Phys. **125**, 074713 (2006)

56. A. Tkatchenko, R.A. Di Stasio, R. Car, M. Scheffler, Phys. Rev. Lett. **108**, 236402 (2012)
57. A.M. Reilly, A. Tkatchenko, J. Phys. Chem. Lett. **4**, 1028 (2013)
58. A. Tkatchenko, A. Ambrosetti, R.A. Di Stasio, Jr., J. Chem. Phys. **138**, 074106 (2013)
59. A. Ambrosetti, A.M. Reilly, R.A. Di Stasio, Jr., A. Tkatchenko, J. Chem. Phys. **140**, 18A508 (2014)
60. F. Göltl, A. Grünesi, T. Bučko, J. Hafner, J. Chem. Phys. **137**, 114111 (2012)
61. T. Bučko, S. Lebègue, J. Hafner, J.G. Ángyán, Phys. Rev. B **87**, 064110 (2013)
62. A. Tkatchenko, D. Alfé, K.S. Kim, J. Chem. Theory Comput. **8**, 4317 (2012)
63. P. Jurečka, J. Šponer, J. Černy, P. Hobza, Phys. Chem. Chem. Phys. **8**, 1985 (2006)
64. P. Giannozzi, S. Baroni, N. Bonini, M. Calandra, R. Car, C. Cavazzoni, D. Ceresoli, G. L. Chiarotti, M. Cococcioni, I. Dabo, A. Dal Corso, S. Fabris, G. Fratesi, S. de Gironcoli, R. Gebauer, U. Gerstmann, C. Gougoussis, A. Kokalj, M. Lazzeri, L. Martin-Samos, N. Marzari, F. Mauri, R. Mazzarello, S. Paolini, A. Pasquarello, L. Paulatto, C. Sbraccia, S. Scandolo, G. Sclauzero, A. P. Seitsonen, A. Smogunov, P. Umari, R. M. Wentzcovitch, J. Phys. **21**, 395502 (2009), http://arxiv.org/abs/0906.2569
65. A. Ferretti, B. Bonferroni, A. Calzolari, M. Buongiorno Nardelli, WanT code. http://www.wannier-transport.org
66. A. Calzolari, N. Marzari, I. Souza, M. Buongiorno, Nardelli. Phys. Rev. B **69**, 035108 (2004)
67. Y.N. Zhang, F. Hanke, V. Bortolani, M. Persson, R.Q. Wu, Phys. Rev. Lett. **106**, 236103 (2011)
68. E. Abad, Y.J. Dappe, J.I. Martnez, F. Flores, J. Ortega, J. Chem. Phys. **134**, 044701 (2011)
69. J.L. Fajín, F. Illas, J.R.B. Gomes, J. Chem. Phys. **130**, 224702 (2009)
70. T.S. Chwee, M.B. Sullivan, J. Chem. Phys. **137**, 134703 (2012)
71. K. Lee, A.K. Kelkkanen, K. Berland, S. Andersson, D.C. Langreth, E. Schröder, B.I. Lundqvist, P. Hyldgaard, Phys. Rev. B **84**, 193408 (2011)
72. K. Lee, K. Berland, M. Yoon, S. Andersson, E. Schröder, P. Hyldgaard, B.I. Lundqvist, J. Phys. **24**, 424213 (2012)
73. M.-S. Liao, C.-T. Au, C.-F. Ng, Chem. Phys. Lett. **272**, 445 (1997)
74. A. Michaelides, V.A. Ranea, P.L. de Andres, D.A. King, Phys. Rev. Lett. **90**, 216102 (2003)
75. A. Hodgson, S. Haq, Surf. Sci. Rep. **64**, 381 (2009)
76. B.W. Heinrich, L. Limot, M.V. Rastei, C. Iacovita, J.P. Bucher, D.M. Djimbi, C. Massobrio, M. Boero, Phys. Rev. Lett. **107**, 216801 (2011)
77. R. Resta, S. Sorella, Phys. Rev. Lett. **82**, 370 (1999)
78. L. He, D. Vanderbilt, Phys. Rev. Lett. **86**, 5341 (2001)
79. C. Brouder, G. Panati, M. Calandra, C. Mourougane, N. Marzari, Phys. Rev. Lett. **98**, 046402 (2007)
80. I. Souza, N. Marzari, D. Vanderbilt, Phys. Rev. B **65**, 035109 (2001)
81. M. Iannuzzi, M. Parrinello, Phys. Rev. B **66**, 155209 (2002)
82. R.J. Maurer, V.G. Ruiz, A. Tkatchenko, J. Chem. Phys. **143**, 102808 (2015)
83. M. Rohlfing, T. Bredow, Phys. Rev. Lett. **101**, 266106 (2008)
84. M. Vanin, J.J. Mortensen, A.K. Kelkkanen, J.M. Garcia-Lastra, K.S. Thygesen, K.W. Jacobsen, Phys. Rev. B **81**, 081408 (2010)
85. N. Stoner, M. Van Hove, S. Tong, M. Webb, Phys. Rev. Lett. **40**, 243 (1978)
86. P. Dai, Z. Wu, T. Angot, S.-K. Wang, H. Taub, S. Ehrlich, Phys. Rev. B **59**, 15464 (1999)
87. G. McElhiney, H. Papp, J. Pritchard, Surf. Sci. **54**, 617 (1976)
88. R.J. Behm, C.R. Brundle, K. Wandelt, J. Chem. Phys. **85**, 1061 (1986)
89. K.D. Gibson, S.J. Sibener, J. Chem. Phys. **88**, 7862 (1988)